

Investigations into the spreading dynamics of a viscoelastic drop on a spherical substrate: Analysis and Experiments

*Sudip Shyam¹, Harshad Sanjay Gaikwad¹, Syed Abu Ghalib Ahmed², Bibek Chakraborty²,
Pranab Kumar Mondal^{*1}.*

*¹Microfluidics and Microscale Transport Processes Laboratory,
Department of Mechanical Engineering, Indian Institute of Technology Guwahati, Assam,
India – 781039*

*²Department of Mechanical Engineering, Tezpur University, Napaam, Assam,
India – 781048*

^{*}Email address: mail2pranab@gmail.com, pranabm@iitg.ernet.in

Abstract

We study the spreading dynamics of a hemispherical elastic non-Newtonian liquid drop on a spherical substrate in the capillary driven regime. We use the simplified Phan–Thien–Tanner (sPTT) model to represent the rheology of the elastic non-Newtonian drop. We consider the droplet to be a crater on a flat substrate to calculate the viscous dissipation near the contact line. Following the approach compatible with the capillary-viscous force balance, we establish the evolution equation for describing the temporal evolution of the contact line during spreading. We show that the contact line velocity obtained from the theoretical calculation matches well with our experimental observations. Also, as confirmed by the present experimental observations, our analysis deems efficient to capture the phenomenon during the late-stage of spreading for which the effect of line tension becomes dominant. An increment in the viscoelastic parameter of the fluid increases the viscous dissipation effect at the contact line. It is seen that the higher dissipation effect leads to an enhancement in the wetting time of the droplet on the spherical substrate. Also, we have shown that the elastic nature of fluid leads to an increment in the dynamic contact angle at any temporal instant as compared to its Newtonian counterpart. Finally, we unveil that the phenomenon of increasing contact angle results in the time required for the complete wetting of drop becomes higher with increasing viscoelasticity of the fluid. This article will fill a gap still affecting the existing literature due to the *unavailability of experimental investigations of the spreading of the elastic non-Newtonian droplet on a spherical substrate*.

I. Introduction

Spreading of liquid drops on solid surfaces is encountered frequently in several natural phenomena such as falling of raindrops in the glass window, movement of drop on lotus leaves to different industrial applications. Among the second, a window of practical applications falls in this paradigm are the coating of a solid object by liquid layers, printing technology, micromixing, painting, and many more.¹⁻³ A wide gamut of practical applications alongside a rich physics involved with the underlying spreading phenomenon has motivated researchers to intensely concentrate as well as systematically interrogate several aspects of the spreading dynamics of liquid drop over solid substrates in recent years.^{1,2,4-7} The dynamical behaviour of the droplet spreading on a solid substrate is indeed fascinating in the capillary driven regime, attributed mainly to the complex interplay between surface tension modulated alteration in contact line velocity and the dissipative energy at the three-phase contact line. This phenomenon becomes further involved under the modulation of surface energy as controlled by the substrate wetting characteristics.^{1,2,8-10}

The underlying physical issues concerned with the spreading of non-Newtonian drops on a solid substrate are more complex. The primary attributable factor behind this facet is the rheology driven modifications of the flow dynamics and its subsequent effect on the contact line motion.¹¹⁻¹³ Taking a note on this aspect, efforts have been directed at the exploration of complicated phenomenon delimited with the spreading of non-Newtonian drops on substrates having different geometrical topographies in recent times.^{1,5,14-17} It is important to mention here that the underlying phenomenon of droplet spreading on the spherical substrates is markedly different from that on the flat substrates, attributable to the intensified effect of *line tension* on the spreading dynamics.^{6,18-22} At low contact angle, the effect of line tension, however small it is, becomes vital on the spreading dynamics of drops on a spherical substrate. As shown by the researchers,¹⁸ a small but non-zero finite magnitude of line tension is an indicative measure for the complete wetting state of drop on a spherical substrate.¹⁸

Majority of the literature referenced above have dealt with the droplet spreading dynamics considering either Newtonian fluid or non-Newtonian fluid with inelasticity on surfaces having different morphologies.^{1,5,14-17} Important to mention, the spreading phenomenon of the elastic non-Newtonian drop, precisely viscoelastic drop, on a spherical substrate is expected to encounter complicated dynamics on account of a number of factors. This complicated dynamical behaviour is primarily triggered by the correlative-cooperative

effect of fluid viscoelasticity on the underlying flow dynamics. It is worth to add here that the spreading of viscoelastic drop on a spherical substrate in the presence of line tension effect, which is more useful for ensuring the complete wetting state of the droplet (late-stage), becomes even more convoluted as the contact-line radius tends to vanish (onset point of singularity). Considering above all aspects, the spreading of elastic non-Newtonian drop on spherical substrate seems to be of vital importance from two different perspectives: first, because of its direct consequence to practical relevance including printing, coating, etc. Second, for the understanding of rich physics involved with the underlying phenomenon. Important to mention, this aspect has not been explored to date as apparent from a comprehensive review of the reported literature in this paradigm.

Here, we investigate the spreading dynamics of a viscoelastic drop on a spherical substrate following a complex theoretical analysis. Also, to substantiate the efficacy of our theoretical model, we perform experiments for the spreading of a viscoelastic drop in the regime compatible with the capillary-viscous force balance. Our theoretical results of the spreading behaviour of the viscoelastic drop match well with the experimental observations. Most importantly, our theoretical model developed in predicting the spreading behaviour of the elastic non-Newtonian drop, which encompasses the class of shear-thinning fluid along with a particular case of the Newtonian droplet, benchmarked with the experimental data will provide a basis for further investigations towards capturing intricate details of the droplet spreading dynamics. *Quite non-intuitively, the theoretical framework developed in this study can accurately predict the behaviour during the late-stage of the spreading, as confirmed by the experimental evidence under identical conditions.*

II. Spreading of viscoelastic drop on a spherical substrate

A. Mathematical modelling

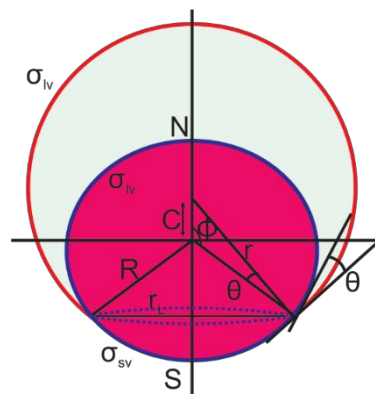


Figure 1 (will appear colour online): The plots depict the schematic of a spherical liquid droplet spreading from the north pole ‘N’ of a spherical substrate towards its south pole ‘S’. The distance

between the center of the droplet and the spherical substrate is given by C . Note that r_L denotes the radius contact line, while θ is the dynamic contact angle, which is related to the half of the central angle ϕ .

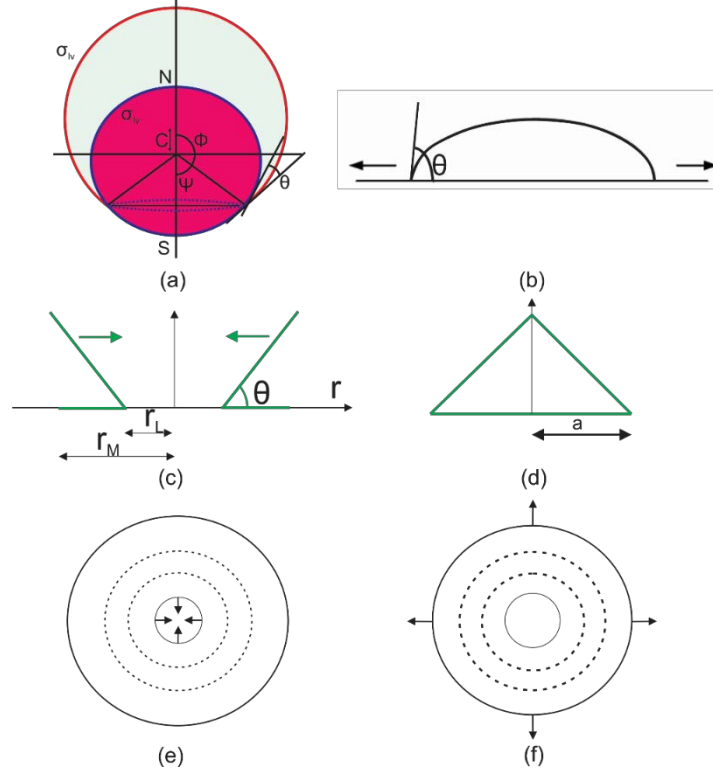


Figure 2 (will appear colour online): (a) Schematic represents the spreading of a droplet on a spherical substrate toward the complete-wetting state. At this stage, the three-phase contact line shrinks towards the south pole S of the spherical substrate; (b) Plot depicts the droplet spreading on a flat substrate. For this particular case, the three-phase contact line expands towards infinity. Thus, the line tension on a spherical substrate plays an opposite role to that on a flat substrate; (C) Schematic represents the crater-shaped model of spreading droplet on a spherical substrate, while (d) shows the cone-shaped model of the droplet on a flat substrate; (e) Plot depicts the bottom view of the spreading droplet, whose contact line shrinks towards south pole S of the spherical substrate, and (d) shows the top view of the spreading droplet whose contact line expands towards infinity on a flat substrate.

We here consider the spreading of a hemispherical elastic non-Newtonian drop on a spherical substrate as schematically shown in Fig. 1. To represent the rheology of the elastic non-Newtonian fluid, we use the simplified Phan-Thien-Tanner (sPTT) model in this analysis. Following this model, we can write the constitutive equation for viscoelastic fluid as^{23,24}

$$f(\text{tr}(\boldsymbol{\tau}))\boldsymbol{\tau} + \lambda \left[\frac{\partial \boldsymbol{\tau}}{\partial t} + \mathbf{u} \cdot \nabla \boldsymbol{\tau} - ((\nabla \mathbf{u})^T \cdot \boldsymbol{\tau} + \boldsymbol{\tau} \cdot \nabla \mathbf{u}) \right] = 2\eta \mathbf{D} \quad (1)$$

In Eq. (1), $\boldsymbol{\tau}$ is the stress tensor, λ is the relaxation time, \mathbf{D} is the deformation rate tensor, $f(\text{tr}(\boldsymbol{\tau}))$ is a function of the trace of the stress tensor, and η is the viscosity coefficient. Before proceeding to outline the detailed analysis of the problem considered in

this study, we would like to mention here that the present analysis focuses on the complete spreading phenomenon, including early-stage and late-stage spreading of the droplet. Important to mention, on account of this aspect, we model the spreading phenomenon of the viscoelastic drop on a spherical substrate by considering a shrinking crater on a flat substrate, as shown through schematic depictions in Fig. 2.^{4,5} We can see from Fig. 1 that, as the droplet is advancing, the three-phase contact line is shrinking towards the south pole ‘S’ of the spherical substrate. Note that, in the crater model, this contact line is depicted by a circle that is shrinking towards a singular point on a flat surface, as shown in Figs. 2(c),(e).

In an effort to capture the flow physics of our interest, including the phenomenon during the late-stage spreading of a viscoelastic drop, we now solve the Cauchy momentum equation.^{14,25} Note that the Cauchy momentum equation for describing the axially-symmetry flow in the regime of low Reynolds number ($Re \ll 1$) takes the following form as:¹⁴

$$-\nabla p + \nabla \cdot \boldsymbol{\tau} = 0 \quad (2)$$

where p is the pressure and $\boldsymbol{\tau} (= \tau_{rz})$ is the shear stress. We use the following boundary conditions to solve Eq. (2) as mentioned below.

$$\left. \begin{array}{l} \text{No shear at the liquid- air interface : } \partial u / \partial \mathbf{n} = 0 \\ \text{No slip at the solid- liquid interface : } \mathbf{n} \times \mathbf{u} = 0 \end{array} \right\} \quad (3)$$

We now look at Eq. (1) and make an effort to obtain the expression of shear stress, which is required to solve for the velocity field of viscoelastic liquid. It is worth mentioning here that our analysis of droplet spreading, consistent with the energy balance approach, largely relies on the accurate prediction of dissipative energy due to viscous dissipation at the contact line. An accurate prediction of dissipative energy at the contact line necessitates the description of liquid velocity in the flow field. Next, we discuss the intermediate steps for the derivation of stress using Eq. (1), essentially to obtain the velocity field in the droplet domain. Note that this exercise will help readers to have a complete understanding of the underlying method adopted in this study. To start with, for the problem under the present investigation, we consider the cylindrical coordinate system with axial symmetry; since the advancement of the crater towards the singular point ‘S’ (South Pole) will be axially symmetric (i.e., $\partial()/\partial\theta = 0$ and $u_\theta = 0$). Now, using Eq. (1), we get,

$$\boldsymbol{\tau} = \begin{pmatrix} \tau_{rr} & \tau_{rz} \\ \tau_{rz} & \tau_{zz} \end{pmatrix} \text{ and } \mathbf{u} = \begin{pmatrix} u_r \\ u_z \end{pmatrix} \quad (4)$$

The deformation rate tensor takes the following form as:

$$\mathbf{D} = \frac{(\nabla u + (\nabla u)^T)}{2} = \begin{pmatrix} \frac{\partial u_r}{\partial r} & \frac{1}{2} \left(\frac{\partial u_r}{\partial z} + \frac{\partial u_z}{\partial r} \right) \\ \frac{1}{2} \left(\frac{\partial u_r}{\partial z} + \frac{\partial u_z}{\partial r} \right) & \frac{\partial u_z}{\partial z} \end{pmatrix} \quad (5)$$

Assuming the flow to be in the creeping flow regime (low Reynolds number flow), which is valid for present analysis as well, and $u_z \approx 0$, we can write the following equations for the problem under consideration as:

$$\left. \begin{aligned} \frac{\partial u_r}{\partial r} &= 0 \\ \frac{\partial \tau_{rr}}{\partial r} &= \frac{\partial \tau_{rz}}{\partial r} = \frac{\partial \tau_{zz}}{\partial r} = 0 \end{aligned} \right\} \quad (6)$$

Now, employing this condition as given in Eq. (6) and upon substituting the expression of $\boldsymbol{\tau}$, u and \mathbf{D} [Eqs. (4) and (5)], the constitutive equation for viscoelastic fluid, as given by Eq. (1), takes the following form:

$$f(\text{tr}(\boldsymbol{\tau})) \begin{pmatrix} \tau_{rr} & \tau_{rz} \\ \tau_{rz} & \tau_{zz} \end{pmatrix} - \lambda \begin{pmatrix} 2\tau_{rz} \frac{\partial u_r}{\partial z} & \tau_{zz} \frac{\partial u_r}{\partial z} \\ \tau_{zz} \frac{\partial u_r}{\partial z} & 0 \end{pmatrix} = 2\eta \begin{pmatrix} 0 & \frac{1}{2} \left(\frac{\partial u_r}{\partial z} \right) \\ \frac{1}{2} \left(\frac{\partial u_r}{\partial z} \right) & 0 \end{pmatrix} \quad (7)$$

From Eq. (7), we obtain the following set of equations as written below.

$$f(\text{tr}(\boldsymbol{\tau}))\tau_{rr} = 2\lambda\tau_{rz} \frac{\partial u_r}{\partial z} \quad (8(a))$$

$$f(\text{tr}(\boldsymbol{\tau}))\tau_{rz} = \eta \frac{\partial u_r}{\partial z} + \lambda\tau_{zz} \frac{\partial u_r}{\partial z} \quad (8(b))$$

$$f(\text{tr}(\boldsymbol{\tau}))\tau_{zz} = 0 \quad (8(c))$$

To mention, for the assumption considered in this analysis, Eqs. 8(a)-(c) as delineated above describe the rheology of viscoelastic fluid consistent with the sPTT model. From Eq. 8(c), we get $\tau_{zz}=0$, since $f(\text{tr}(\boldsymbol{\tau}))=0$ will give a trivial solution. Now substituting $\tau_{zz}=0$ [from Eq. 8(c)] in Eq. 8(b), we get the following equation.

$$f(\text{tr}(\boldsymbol{\tau}))\tau_{rz} = \eta \frac{\partial u_r}{\partial z} \quad (9)$$

The function of the trace of the stress tensor is ideally an exponential function. However, for very low shear stress magnitude, this function can be approximated using its linear form as given below.^{14,26}

$$f(\text{tr}(\boldsymbol{\tau})) = 1 + \frac{\varepsilon\lambda}{\eta} \tau_{rr} \quad (10)$$

where ε is the extensibility parameter used to model the extensional viscosity of the fluid; instead, this parameter to be precise limits the extensional viscosity, η is the viscosity, and λ is the relaxation parameter. Now, we look at Eqs. 8(a) and (9) to obtain the following,

$$\tau_{rr} = \frac{2\lambda}{\eta} \tau_{rz}^2 \quad (11)$$

Using Eqs. (9), (10) and (11), we obtain another form of the governing equation, as written below.

$$\tau_{rz} \left(1 + \frac{2\varepsilon\lambda^2}{\eta^2} \tau_{rz}^2 \right) = \eta \frac{\partial u_r}{\partial z} \quad (12)$$

The above equation [Eq. 12] is the final form of the governing equation for describing the flow dynamics of the viscoelastic fluid pertinent to this analysis.^{14,26} Using this constitutive relation, we solve the Cauchy momentum equation as described in Eq. (2) essentially to obtain the velocity distribution in the droplet volume. We next write the Cauchy momentum equation for low Reynolds number and axially-symmetric flow as:

$$-\frac{dp}{dr} + \frac{\partial \tau_{rz}}{\partial z} = 0 \quad (13)$$

Now using this equation [Eq. (13)], we calculate the order of magnitude of the shear stress τ_{rz} by appealing to the condition of zero stress condition at the free surface, i.e., $\tau_{rz}|_{z=h(r)} = 0$.

The expression of shear stress reads as:

$$\tau_{rz} = \frac{dp}{dr} (z - h) \quad (14)$$

where $h(r)$ is the height of the liquid-air surface from the substrate at the distance r from the droplet center [Fig. 2(c)]. Using Eqs. (12), (14) and no-slip (dynamic boundary condition) condition at the surface, i.e., $u_r|_{z=0} = 0$ we get,

$$u_r = \frac{1}{\eta} \frac{dp}{dr} \left[\left(\frac{1}{2} \left\{ (z-h)^2 - h^2 \right\} \right) + \left(\frac{2\varepsilon\lambda^2}{4\eta^2} \right) \left(\frac{dp}{dr} \right)^2 \left\{ (z-h)^4 - h^4 \right\} \right] \quad (15)$$

Note that for $\lambda=0$, the velocity distribution described in Eq. (15) confirms the velocity field for a Newtonian fluid on spherical substrates.⁵ It may be mentioned here that Eq. (15) governs the relation among the flow parameters, i.e., the fluid velocity (u_r) and the fluid properties, i.e., the viscoelastic parameters λ , and the extensibility parameter ε . On a related note, we would like to mention here that the aforementioned viscoelastic parameters can be grouped together and represented by a non-dimensional parameter. This non-

dimensional parameter is termed as the Deborah number or Weissenberg number.²⁶ Now from the order of magnitude analysis of two different terms in Eq. (13), we can write the following as:

$$\frac{dp}{dr} \sim \frac{\eta u_{ref}}{h^2} \quad (16)$$

where u_{ref} is the late-stage spreading (precisely, the contact line velocity) velocity. The pressure gradient will have a negative value, which implies that the proportionality constant has to be negative. Moreover, since we are equating the order of the magnitude of the terms in Eq. (13), this proportionality constant will be unity. Important to mention, this proportionality constant will assume different values for the varying magnitude of the fluid viscoelasticity. Note that with a change in the relaxation time of the fluid, the viscoelasticity changes as realized by the different values of the Deborah number in the dimensionless form. Now, Eq. (15) can be written in the following dimensionless form as:

$$\bar{u}_r = \frac{-1}{2} \left[\left\{ 1 - (1 - \bar{z})^2 \right\} \left\{ 1 + \varepsilon De^2 \left(1 + (1 - \bar{z})^2 \right) \right\} \right] \quad (17)$$

where $De (= \lambda u_{ref}/h)$ is the Deborah number, $\bar{u}_r (= u_r/u_{ref})$ is the dimensionless velocity and $\bar{z} (= z/h)$ is dimensionless coordinate. As mentioned before, the Deborah number is a dimensionless number signifying the elasticity of the fluid.²⁶ It is worth mentioning here that the expression of velocity distribution as given in Eq. (17) for a limiting case of $De = 0$ matches well with the expression reported by Iwamatsu for Newtonian fluids ($n = 1$).⁵ Since we consider the energy balance approach in this study to obtain the droplet spreading behaviour, we now calculate the viscous dissipation in the fluid drop, including the one at the contact line. The expression of the viscous dissipation can be written as:

$$\dot{D}_{vis,drop} = \int_{\Omega} \Phi d\Omega \quad (18)$$

Here, $\Phi (= \tau_{rz} (du_r/dz))$ is the viscous dissipation per unit volume of the drop $d\Omega$ and Ω is the total volume.^{14,27} For axisymmetric flow, which is the case for this analysis as well, the viscous dissipation can be written as:¹⁴

$$\dot{D}_{vis,drop} = \int_{r_L + \Delta r}^{r_M} \int_0^{2\pi} \int_0^h \tau_{rz} \left(\frac{du_r}{dz} \right) dz d\phi r dr \quad (19)$$

It is worth mentioning here that to avoid the problem of singularity at $r = 0$, we here introduce the upper bound r_M and the lower bound r_L with the cut-off radius Δr . Note that

Eq. (19) can be integrated to obtain the explicit expression of viscous dissipation. We can calculate τ_{rz} from Eqs. (14) and the velocity gradient from Eq. (17). Below, we write the expression of (du_r/dz) , which can be obtained from Eq. (17) as:

$$\frac{d\bar{u}_r}{d\bar{z}} = - \left[(1 - \bar{z}) \left\{ 1 + 2\varepsilon De^2 (1 - \bar{z})^2 \right\} \right] \quad (20)$$

Now, substituting the expressions of τ_{rz} and (du_r/dz) in Eq. (19) and then integrating this equation [Eq. (19)] with respect to z and ϕ , we will get the expression of the viscous dissipation. The form of viscous dissipation reads as:

$$\dot{D}_{vis,drop} = 2\pi\eta u_{ref}^2 \left[\frac{1}{3} + \frac{2\varepsilon De^2}{5} \right] \int_{r_L+\Delta r}^{r_M} \frac{1}{h} r dr \quad (21)$$

Since we have considered a crater model in this analysis, we can assume the meniscus of the viscoelastic drop, as shown by Figs. 2(c), (e) to be axially-symmetric wedged-shaped. Now, owing to this consideration, we can write the following expression for a small contact angle θ as:

$$h(r) = \tan \theta (r - r_L) \ll \theta (r - r_L) \quad \forall \text{ small } \theta \quad (22)$$

Further integration of Eq. (21) yields the following final expression of the viscous dissipation and given as:

$$\dot{D}_{vis,drop} = \frac{2\pi\eta u_{ref}^2 r_L \kappa}{\theta} \left(\frac{1}{3} + \frac{2\varepsilon De^2}{5} \right) \quad (23)$$

The term κ appearing in Eq. (23) can be written below:

$$\kappa = \Lambda - 1 + \ln(\Lambda - 1) - \delta - \ln \delta \quad (24)$$

where $\Lambda = r_M/r_L$ and $\delta = \Delta r/r_L$. Note that Eq. (24) shows a well-known singularity, which is $\kappa \sim \ln \delta$. Important to mention here, this singularity will occur as $\delta \rightarrow 0$. But for the present problem of spreading on a spherical substrate where $r_L \rightarrow 0$, this singularity ($\delta \rightarrow 0$) will not be important, and hence, it will not occur. Next, we calculate the thermodynamic force (capillary force), which also includes the free energy at the three-phase (fluid-fluid-solid) contact line. Below we write the expression of the thermodynamics force (capillary force per unit length) as:⁶

$$f_{cap} = \sigma_{lv} (\cos \theta_Y - \cos \theta) - \frac{\tilde{\lambda}}{R \tan \phi} \quad (25)$$

In Eq. (25), σ_{lv} is the liquid-air surface tension, $\tilde{\lambda}$ is the line tension at the three-phase contact

line,⁶ θ_Y is Young's contact angle at equilibrium, and ϕ is half of the central angle, as shown in Fig. 2(a).

Now, the energy balance condition at the contact line with the radius r_L leads to the following equation as written below:¹⁴

$$2\pi r_L f_{cap} u_{avg} = \dot{D}_{vis, drop} \quad (26)$$

Note that $u_{ref} \sim u_{avg}$. Now using Eqs. (19)-(20) and (23)-(24), we can re-write Eq. (26) in the form as given below:

$$\sigma_{lv} \left[(\cos \theta_Y - \cos \theta) - \frac{\tilde{\lambda}}{\tan \phi} \right] = \frac{\eta u_{ref} \kappa}{\theta} \left(\frac{1}{3} + \frac{2\varepsilon D e^2}{5} \right) \quad (27)$$

In Eq. (27), $\tilde{\lambda} = \lambda / (\sigma_{LV} R)$ is the scaled line tension relative to liquid-air interfacial tension σ_{lv} .⁴⁻⁶ As already mentioned, our analysis takes into account the phenomenon during the late-stage spreading of an elastic non-Newtonian drop on a spherical substrate. We here make an effort to investigate the variation of the contact angle on a hydrophilic surface and its effect on the variation of contact-line velocity, as discussed next. For late-stage spreading on a hydrophilic substrate, we will consider $\theta \ll 1$ and $\theta_Y \ll 1$, while the angle ψ following its description in Fig. 2(a) can be written as:

$$\left. \begin{aligned} \psi|_{\text{late-stage}} &= (\pi - \phi) \rightarrow 0 \\ r|_{\text{late-stage}} &\rightarrow r_0 \end{aligned} \right\} \quad (28)$$

Note that r_0 in the above equation is the radius of the droplet as it completely wets the spherical substrate of radius R , i.e., $r_0 > R$. Hence, in a complete wetting condition (i.e., $\theta_Y = 0^\circ$), we can obtain the droplet volume $V_0 = (4\pi/3)(r_0 - R)^3$. Also, having a closer look at Fig. 1, we get the following expression as written below.

$$\tan \phi = \frac{r \sin \theta}{R - r \cos \theta} \quad (29)$$

Now using Eq. (28) and including the consideration leading to the late-stage spreading behaviour in this analysis, we obtain the following expression as:

$$\tan \phi \approx -\psi \rightarrow \frac{-r_0}{(r_0 - R)} \theta \quad (30)$$

Hence, the radius of the contact line (r_L) can be written as (cf. Fig 1 for a clearer view):

$$r_L = R \sin \phi \simeq R\psi \simeq \frac{r_0}{(r_0 - R)} R\theta \quad (31)$$

Now using Eqs. (28)-(31), the equation governing the spreading dynamics (energy balance condition), i.e., Eq. (27), which includes the late-stage scenarios as well, takes the following form.

$$\theta \left[\frac{1}{2} (\theta^2 - \theta_Y^2) + \frac{r_0 - R}{r_0 \theta} \tilde{\lambda} \right] = \frac{\eta u_{ref} \kappa}{\sigma_{LV}} \left(\frac{1}{3} + \frac{2\varepsilon De^2}{5} \right) \quad (32)$$

As the contact angle θ during late-stage spreading is very low, the spreading velocity (precisely, the contact line velocity) on the spherical substrate can be written as:

$$u_{ref} \sim \frac{d}{dt}(R\phi) = \frac{d}{dt}(-R\psi) = -\frac{r_0}{(r_0 - R)} R\dot{\theta} \quad (33)$$

Now, substituting u_{ref} in Eq. (32), we get another form as written below.

$$\theta \left[\frac{1}{2} (\theta^2 - \theta_Y^2) + \frac{r_0 - R}{r_0 \theta} \tilde{\tau} \right] = -\frac{\kappa \eta}{\sigma_{LV}} \left(\frac{1}{3} + \frac{2\varepsilon De^2}{5} \right) \frac{r_0}{r_0 - R} R\dot{\theta} \quad (34)$$

We proceed one step further to cast Eq. (34) into the following form as given by,

$$\Gamma \left(\frac{1}{3} + \frac{2\varepsilon De^2}{5} \right) \frac{d\theta}{dt} + \theta \left[\frac{1}{2} (\theta^2 - \theta_Y^2) + \frac{r_0 - R}{r_0 \theta} \tilde{\tau} \right] = 0 \quad (35)$$

The coefficient $\Gamma = \frac{\kappa \eta}{\sigma_{lv}} \left(\frac{r_0}{r_0 - R} \right) R$ is the time scale of spreading. As clearly evident from the expression, this coefficient depends on the radius of the substrate R , and the droplet volume V_0 having radius r_0 $[V_0 = (4\pi/3)(r_0 - R)^3]$. It needs to be mentioned here that, for $De = 0$, Eq. (35) reduces to the equation, governing the spreading dynamics of the Newtonian drop on the spherical substrate.^{4,6}

$$\frac{d\theta}{dt} = -\frac{\theta}{\Gamma} \left[\frac{1}{2} (\theta^2 - \theta_Y^2) + \frac{r_0 - R}{r_0 \theta} \tilde{\tau} \right] \quad (36)$$

Now for the complete wetting case, i.e., for an underlying spreading phenomenon on a completely hydrophilic surface, as realizable by Young's contact angle $\theta_Y = 0$, and by neglecting the line tension effect ($\tilde{\lambda} = 0$), we can write Eq. (36) in the following form.

$$\theta = \theta_0 \left(1 + \theta_0^2 (t/\Gamma) \right)^{-1/2} \quad (37)$$

where θ_0 is the initial contact angle at $t = 0$. Now we can write the time evolution of dynamic contact angle as:

$$\theta \propto (t/\Gamma)^{-1/2} \quad (38)$$

It is worth mentioning here that Eq. (32) as obtained for the limiting condition of $De \rightarrow 0$ is showing similarity with the reported equation governing the spreading of Newtonian drop ($n = 1$) on the spherical substrate.^{5,6} We would like to mention here that for the smaller value of dynamic contact angle ($\theta \rightarrow 0$), the contributory effect of line tension [cf. Eq. (34); the second term of LHS of this equation becomes effective as $\theta \rightarrow 0$] on the underlying spreading dynamics becomes important. Accounting this aspect, we solve Eq. (35) using the Runge-Kutta method for an initial contact angle $\theta_0|_{t=0} \sim 1$. Also, we consider ring spreading on a complete hydrophilic substrate ($\theta_y = 0$), and the effect of line tension is taken comparatively in a smaller range.

B. Experimental details

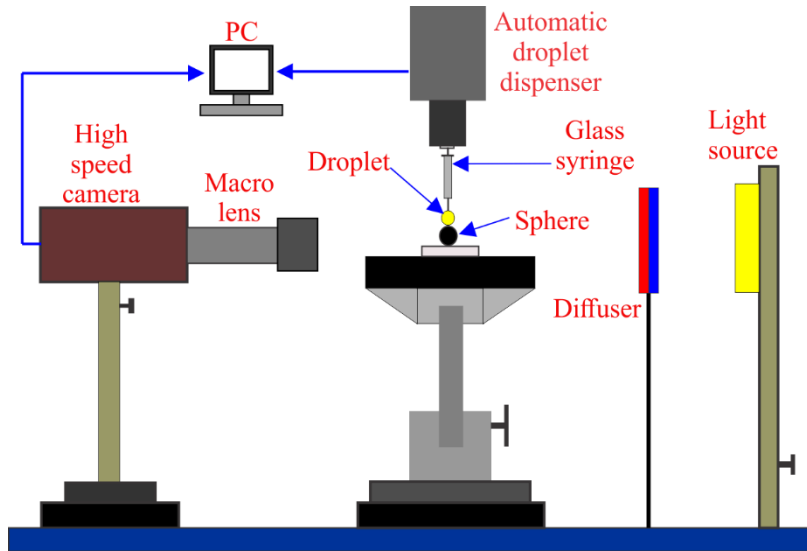


Figure 3 (will appear colour online): Schematic of the experimental set-up. The set-up includes the following: Macro lens, high-speed camera, automatic droplet dispenser, spherical substrate placed on the test plane, diffuser, light source, glass syringe.

To verify the accuracy of the theoretical model outlined in the preceding section, we perform experiments on the spreading of a viscoelastic drop on a spherical substrate. In particular, the experimental observations substantiates the credibility of our theoretical model in describing the phenomenon during the late-stage of the spreading as well. We show, in Fig. 3, the experimental set-up schematically. Droplets of a predefined size ($V_0 = 3\mu l$) are generated using a 250 μl glass syringe (Make: Hamilton), which is further controlled by a precision drop dispenser mechanism (Make: Apex instruments), integrated with the circuit.

We capture the spreading dynamics at 50 frames/s (1280×800 pixels resolution) by using a high-speed camera (Make: Phantom), coupled with a macro lens (Make: Nikkor, Nikon) of focal length 105 mm. For the optical arrangement in the circuit, we use a brightness controlled white LED light (Make: Holmarc Opto-Mechatronics) along with a diffuser as a backlight. Notably, for the present experiments, we use the solution of 5% Polyisobutylene (PIB) in Tetradecane (C14) as the viscoelastic fluid. A polished stainless steel ball of 3.85mm diameter is used as the spherical substrate, as shown in the schematic of Fig. 3. The cleaning protocol is such that the substrate is initially cleaned with acetone and then dried in a hot air oven at 120°C for 20 minutes. Note that all the experiments are conducted in the capillary controlled spreading regimes.

III. Synthesis and characterization of the viscoelastic fluid

Here we briefly discuss the synthesis and characterization of the viscoelastic fluid used in this study. For the preparation of the viscoelastic fluid, we chemically synthesize a solution of Polyisobutylene (PIB-Vistanex L120, $M_w=1 \times 10^6$) in tetradecane ($\text{C}_{14}\text{H}_{30}$ -Newtonian solvent). Small pieces of PIB (5%, w/w) were thoroughly mixed in tetradecane (solvent) with the help of a magnetic stirrer (Make: Tarsons). The approximate duration of the stirring process was around five days. Following this, the prepared solution was continuously rotated on a rolling machine (Make: LMBR500) for one week. It is important to mention that the ambient temperature throughout the chemical synthesis process was maintained around 25°C . Also, note that at this particular volume fraction (5%, w/w) of PIB in the prepared solution, Phan-Thien-Tanner model (PTT model) was found to be the best fitted theoretical model.^{28–31} Accordingly, the following parameters of the PTT model were used in the present study: viscosity $\eta=1.424$ Pa.s, relaxation time $\lambda = 0.06$ sec, and extensibility parameter $\varepsilon=0.05$. Following the seminal work of Iwamatsu,^{6,32} the surface tension and the line tension of the prepared PIB/C14 solution were found to be around 22 mN/m and 0.02 mN/m, respectively. Now, using all the values mentioned above, we calculate the reference scales, i.e., the velocity scale (u_{ref}) and the length scale (h) to be $u_{ref} \sim 10^{-3}$ m/sec, and $h \sim 10^{-5}$ m, respectively. It is worth mentioning here that for these reference scales and using the parameters mentioned above; we calculate the magnitude of the Capillary number (Ca) and the viscoelastic parameter (εDe^2) to be of the order of $O[10^{-3}]$ and $O[10^{-1} - 10^0]$.

IV. Results and Discussion

A. Experimental observations of the spreading: Benchmarking the theoretical model

As an important objective of the present endeavor, we here make an effort to establish the effectiveness of our theoretical model in predicting the droplet spreading behavior on a spherical substrate by comparing with the experimental observations. In doing so, we show in Fig. 4(a) the temporal variation of $d\bar{h}/d\bar{t}$ during the spreading process, while the snapshots of the droplet spreading process on the spherical substrate captured at various time instants are shown in Fig. 4(b). The markers in Fig. 4(a) are used to represent the experimental results, while the straight line shows the results obtained from the theoretical calculations. As already mentioned, \bar{h} is the height (dimensionless) of the liquid-air surface from the substrate. Note that, for this validation, we consider the spreading of a viscoelastic drop having viscoelasticity as represented by $\varepsilon De^2 = 0.1$. Next, we discuss the notable points observed from the evolution of $d\bar{h}/d\bar{t}$ in Fig. 4(a) as follows. During the initial stages of spreading, the temporal gradient is high, and we observe a sharp change in the temporal evolution of the height. We would like to mention here that the three-phase contact line plays an important role in governing the flow dynamics in the capillary-driven spreading phenomenon. In this initial regime of the spreading, the capillary force governs the flow by dominating its effect over the viscous forcing and results in a higher velocity of the contact line. It is because of the higher contact line velocity; we observe a sharp gradient of $d\bar{h}/d\bar{t}$ during the initial stage. We observe different scenarios at a later stage of the spreading. Note that, as the time grows (late-stage), the droplet spreads on the substrate following a balance between the capillarity and the viscous stresses. Prominently, compatible with a capillary-viscous force balance, the contact line velocity slowed down during the late-stage of the spreading as supported by the snapshots presented in Fig. 4 (see the images from 26.8 sec onwards). Precisely, slower movement of the contact line velocity results in an insignificant change in the height with time, as witnessed by the constant value of $d\bar{h}/d\bar{t}$ in Fig. 4(a) and the images (from 26.8 sec onwards) in Fig. 4(b). The inset in Fig. 4(a) plots the variation of $d\bar{h}/d\bar{t}$, during the late stage of the spreading process. Quite remarkably, the calculations predicted by the present theoretical framework are in coherence with our observations made from our experimental investigations, as witnessed by Fig. 4(a). This observation justifies the credibility of our theoretical model developed in this study in predicting the spreading dynamics of an elastic non-Newtonian fluid.

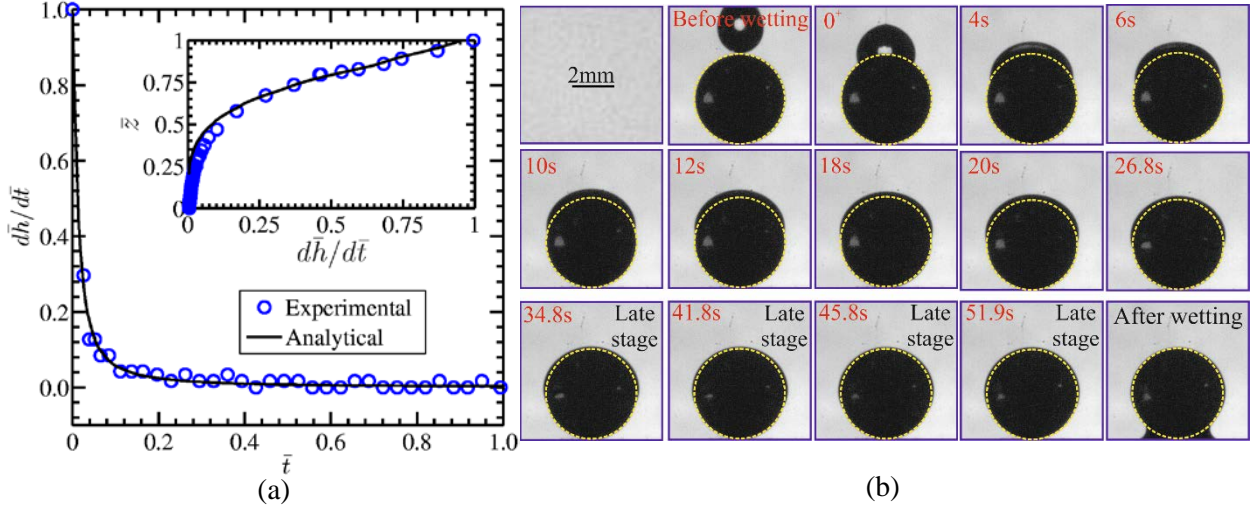


Figure 4 (will appear color online): (a) Plot shows the experimental and theoretical variation of $d\bar{h}/d\bar{t}$ along the temporal direction. The inset shows the variation of $d\bar{h}/d\bar{t}$ along \bar{z} during the droplet spreading process on the spherical substrate; (b) Snapshots show the temporal evolution of the droplet spreading phenomenon of the viscoelastic fluid on the spherical substrate. The dotted yellow circle demarcates the boundaries of the spherical substrate. For the present case, the value of εDe^2 is around 0.1.

B. Effect of fluid viscoelasticity on the spreading dynamics

1. The variation of the flow velocity: Contact line dynamics

Before going for the discussion of the pertinent results as presented in this section, it may be mentioned here that increasing the magnitude of the relaxation time (λ) (equivalently for the higher Deborah number in the dimensionless form) enhances the elastic nature of the fluid. Because of this increasing elastic nature, the fluid will behave more like a solid than a liquid for higher Deborah number.³³ So, for the viscoelastic fluids with higher viscoelasticity as realized by the higher value of εDe^2 (as relaxation time increases), the spreading ability decreases. From Eq. 11, it is seen that the normal stress component (τ_{rr}) and relaxation time (λ) are related by the expression $\tau_{rr} = (\tau_{rz})^2 2\lambda/\eta$. Following this expression, it is evident that τ_{rr} is directly proportional to the relaxation time of the fluid. As a consequence, the flow rate becomes higher for viscoelastic fluid as compared to that of a Newtonian fluid, while increasing relaxation time (λ) is expected to enhance the flow rate as well. We attribute this effect to the increase in the shear-thinning behavior of the fluid with increasing viscoelasticity (εDe^2).²⁶ Important to mention, the shear-thinning effect, which becomes stronger with increasing (εDe^2), will increase the shear rate as can be seen from Eqs. (16) and (17). Considering the non-dimensional velocity gradient as in Eq. (19), we can get

$du_r/d\bar{z} = -\left[(1-\bar{z})\left\{1+2\epsilon De^2(1-\bar{z})^2\right\}\right]$. We now make an effort to represent this equation graphically in Fig. 5, wherein the non-dimensional velocity gradient is plotted with a change in droplet height \bar{z} (non-dimensional) for different values of ϵDe^2 .

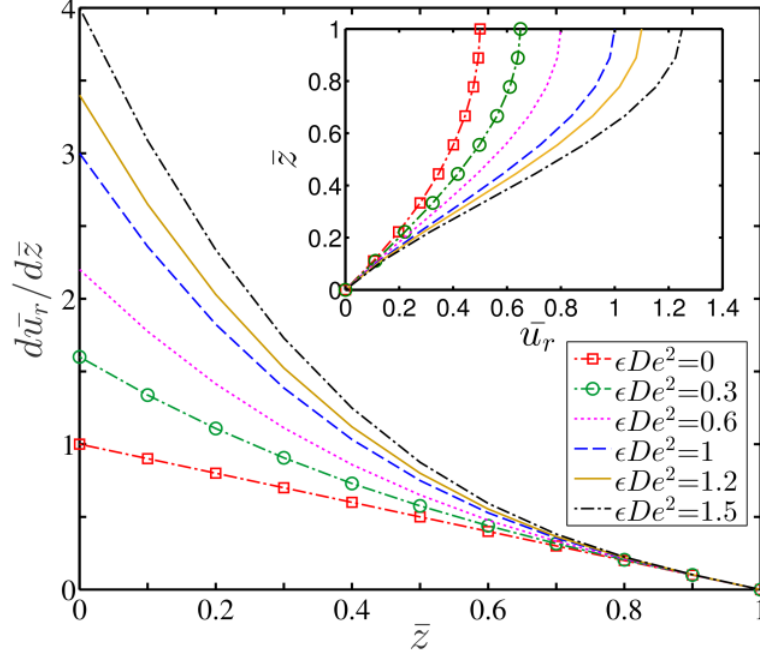


Figure 5 (will appear colour online): Plot showing the variation in velocity gradient (dimensionless) versus droplet height, obtained for different values of ϵDe^2 . As shown in the inset, with increasing viscoelasticity of the fluid as realized by the increasing value of ϵDe^2 , fluid velocity in the droplet domain becomes higher due to the higher shear-thinning effect of the fluid. The higher fluid velocity leads to an increment in the velocity gradient.

From Fig. 5, it is seen that the shear rate at the substrate ($\bar{z} = 0$) increases with the increasing the magnitude of the viscoelastic parameter. Also, one can find from Fig. 5 that the Newtonian fluid will have the least velocity gradient in the droplet flow field, while the magnitude of the velocity gradient becomes higher for the larger viscoelasticity of the fluid. In the capillary driven regime, the higher flow velocity of the viscoelastic fluid, that too becomes higher with increasing magnitude of ϵDe^2 (see inset of Fig. 5), leads to a higher shear rate in the droplet domain. From the definition given in Eq. (17), viscous dissipation can be related as $\phi = \tau_{rz}(du_r/dz)$, and hence, an increase in velocity gradient is expected to increase in the viscous dissipation. Since we are considering the energy balance approach in this study, which is consistent with the hydrodynamic model as well^{2,14}, the effect of viscous dissipation becomes the only opposing factor for the capillary driven spreading in the absence of friction (MKT model).^{1,3,34} As mentioned before, an increase in the viscoelasticity of the fluid increases the viscous dissipation effect following enhancement in the magnitude of the

velocity gradient therein. Notably, this augmented viscous dissipation effect leads to an increase in the magnitude of the dynamic contact angle (cf. Fig. 6(a) in the next subsection). As a consequence of this phenomenon, the time required for the complete wetting of the substrate becomes more than too is observed from Fig. 6(a). Important to mention here that the flow velocity in the droplet domain, as shown in the inset of Fig. 5, can be approximated to the contact line velocity, since our analysis is focused on the capillary controlled spreading of the drop. Quite notably, the velocity in the droplet flow field, as shown in the inset of Fig. 5, shows similar qualitative behaviour with our experimental observations, as shown in the inset of Fig. 4(a). This qualitative observation supports the efficacy of our theoretical model in predicting the droplet spreading dynamics, including the phenomenon during late-stage. Although the spreading dynamics on the spherical substrate is expected to be different than that on a flat surface, the effect of the viscoelasticity will always try to reduce the spreading rate as discussed in the forthcoming section in greater detail.

2. The variation of the dynamic contact angle: A perspective of complete wetting

We depict in Fig. 6(a) the variation in dynamic contact angle $\bar{\theta}$ (dimensionless: normalized with the initial contact angle $\theta_0|_{t=0} = 0$; see Eq. (36)) versus the non-dimensional time, obtained for different values of the viscoelastic parameter. Note that to demarcate the effect of viscoelasticity on the underlying spreading behaviour, we plot in Fig. 6(a) the variation obtained for the limiting case of $\varepsilon De^2 = 0$, i.e., for Newtonian fluid as well. From the variation portrayed in Fig. 6(a), it is seen that at any temporal instant, the dynamic contact angle of the viscoelastic drop is higher than that of a Newtonian liquid drop. Moreover, the dynamic contact angle increases with increasing viscoelastic behaviour (εDe^2) of the fluid which is observed from Fig. 6(a) as well. Important to mention, we consider the capillary number to be of an order of $Ca \sim 10^{-3}$ in this analysis, implicating the underlying phenomenon of spreading to be compatible with capillary-viscous force balance. An increase in the viscoelastic parameter, as realized by an increase in solute concentration will increase the shear-thinning nature of the fluid. It is worth adding here that, for a given strength of the surface tension force (the capillary number is fixed), the fluid velocity will increase with increasing the shear-thinning nature of the fluid as the effective viscosity of the fluid decreases. We have discussed the variation in fluid velocity as well as its gradient in the droplet flow field, obtained with a change in the viscoelastic parameter in the next subsection. We mention here that because of this relatively higher shear-thinning nature of the

fluid with increasing the magnitude of viscoelasticity, the dissipative effect gets strengthened. On account of this higher viscous dissipation, the spreading rate will decrease, and this phenomenon will result in an increment in the dynamic contact angle, as seen in Fig. 6(a). Important to observe, because of this decrement in spreading rate, time enquired for completely wetting the spherical substrate will be larger for a higher value of ϵDe^2 as witnessed in Fig. 6(a).

We further make an effort in Fig. 6(b) to compare our results with the results of the reported analysis in the paradigm of droplet spreading dynamics. Important to mention, our theoretical results in the limiting case, i.e., for $\epsilon De^2 = 0$, signifying the Newtonian fluid behaviour, successfully verify the theoretical results of Iswamatsu⁵ in both the regimes (early as well as late-stages) of the spreading. Note that the spreading behaviour of a Newtonian drop on a spherical substrate is discussed in the reported paper⁵.

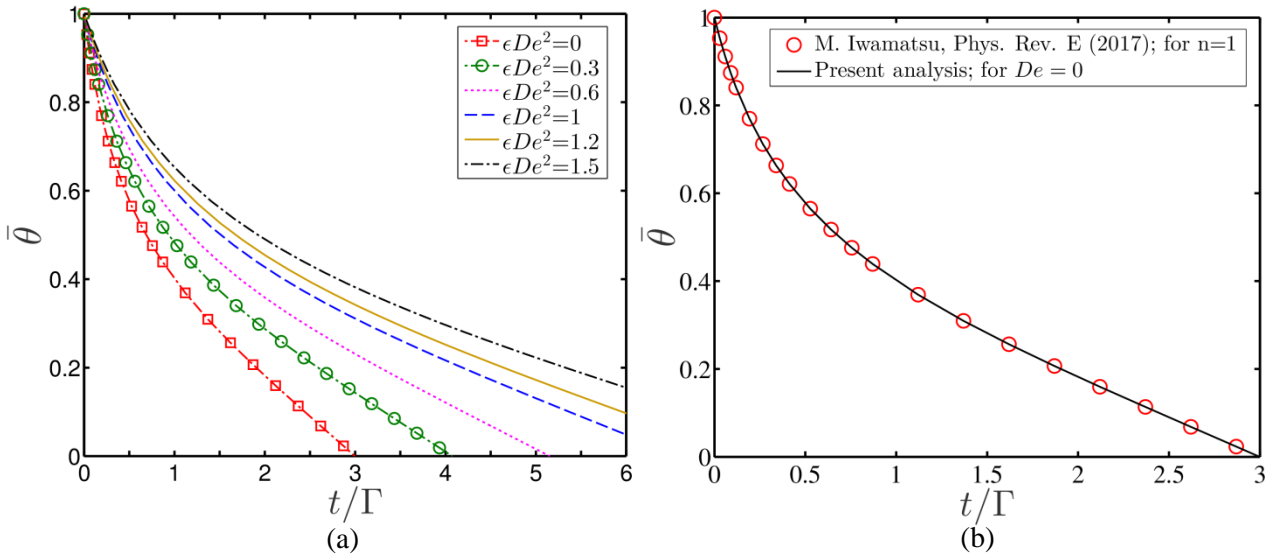


Figure 6 (will appear colour online): (a) Plot showing the temporal variation of contact angle (dimensionless: normalized with initial contact angle $\bar{\theta}|_{t=0} = 1$) for different values of ϵDe^2 . With increasing viscoelasticity of the fluid as realized by the increasing value of ϵDe^2 , the complete wetting time of the surface becomes higher. (b) Plot showing the temporal variation of contact angle (dimensionless: normalized with initial contact angle $\bar{\theta}|_{t=0} = 1$). The solid line represents the variation obtained from the present analysis in the limiting case of $De = 0$, while the ‘O’ markers are used to indicate the results reported by Iswamatsu.⁵

Notable findings of the present endeavour include the development of a model for studying elastic effect modulated spreading dynamics of a non-Newtonian drop on the spherical substrate and subsequent benchmarking of the model with the experimental results. This article will fill a gap on ‘the unavailability of experimental investigations of droplet spreading on a spherical substrate’ still affecting the existing literature in this paradigm.

C. Spreading dynamics: Flat substrate versus spherical substrate

It is important to mention here that, for the spreading phenomenon on a flat surface, the radius of the three-phase contact line expands to infinity. Because of this, the line tension effect becomes unimportant for the underlying spreading on a flat substrate, and its magnitude is taken as negative following the reported value.²¹ On the contrary, for the spreading phenomenon on the spherical substrate, the radius of contact line shrinks, and the curvature diverges (see Fig. 2(a)). Owing to this effect, to achieve the complete wetting stage, the magnitude of line tension must be positive for a spherical substrate.⁶ It may be mentioned in this context here that, for the Newtonian liquid drop, the spreading exponent is 1/10 for flat surface (tanner law) and 1/2 for the spherical substrate.^{1,4,5,35} Also, as reported in the literature, the dynamic contact angle and spreading exponent are co-related as $\theta \propto t^{-\alpha}$, where α is the spreading exponent. Since $\alpha_{sphere} > \alpha_{flat}$, the spreading rate for the Newtonian liquid drop is faster on the spherical substrate as compared to that on a flat substrate. However, due to the effect of fluid elasticity as considered in this analysis, we show that the spreading rate of a viscoelastic liquid drop, in sharp contrast to that of the Newtonian liquid drop, will decrease on both the surfaces. In particular, we demonstrate in this analysis that the spreading rate for both the surfaces (flat as well as spherical) will decrease for the higher viscoelastic behaviour of the fluid. We attribute this phenomenon to the effect of the shear-thinning nature of the fluid, which becomes stronger with increasing the magnitude of the viscoelasticity parameter.

IV. Conclusion

We have developed a hydrodynamic model, consistent with the energy balance approach, to predict the spreading dynamics of a viscoelastic liquid drop on a spherical substrate. To represent the rheology of the viscoelastic fluid, we have considered a simplified Phan–Thien–Tanner (sPTT) model. By comparing the theoretical predictions with our experimental results, we have established that the present modelling framework can successfully predict the phenomenon both in the early and late stages of the spreading. To calculate the viscous dissipation at the contact line, we have modelled the droplet spreading to be a shrinking crater on the flat substrate. Considering the applicability of our model in describing the phenomenon during the late-stage of spreading on a spherical substrate, the magnitude of line tension, in sharp contrast to its negative value for the spreading on a flat surface, is taken as positive necessarily to achieve the complete spreading. We have unveiled that the velocity in the droplet flow field, which can be well-approximated to the contact line

velocity in the capillary driven regime, shows similar qualitative behaviour with our experimental observations. Also, we have established the expression of the dynamic contact angle for the spreading of viscoelastic drop on a spherical substrate compatible with the capillary-viscous forcing regime. We have shown that the elastic nature of viscoelastic fluid leads to an increment in the dynamic contact angle at any temporal instant as compared to its Newtonian counterpart. Finally, we have shown that the phenomenon of increasing contact angle results in the enhancement in the complete wetting time of viscoelastic drop having higher viscoelasticity. We believe that the present analysis may have far ranging consequences towards the long-awaited demand of experimental investigations of the spreading of the elastic non-Newtonian droplet on a spherical substrate

Acknowledgment

PKM acknowledges the financial grants obtained from DST-SERB through project No ECR/2016/000702/ES. Authors acknowledge Microfluidics Laboratory, IIT Guwahati for the experimental facilities.

References

- (1) Rafai, S.; Bonn, D.; Boudaoud, A. Spreading of Non-Newtonian Fluids on Hydrophilic Surfaces. *J. Fluid Mech.* **2004**, *513*, 77–85.
- (2) de Ruijter, M. J.; De Coninck, J.; Oshanin, G. Droplet Spreading: Partial Wetting Regime Revisited. *Langmuir* **1999**, *15* (6), 2209–2216.
- (3) Tanner, L. H. The Spreading of Silicone Oil on Horizontal Surfaces. *J. Phys. D Appl. Phys.* **1979**, *12* (1838), 1473–1485.
- (4) Iwamatsu, M. Spreading Law on a Completely Wettable Spherical Substrate: The Energy Balance Approach. *Phys. Rev. E* **2017**, *95* (5), 052802.
- (5) Iwamatsu, M. Spreading Law of Non-Newtonian Power-Law Liquids on a Spherical Substrate by an Energy-Balance Approach. *Phys. Rev. E* **2017**, *96* (1), 012803.
- (6) Iwamatsu, M. Line Tension and Morphology of a Sessile Droplet on a Spherical Substrate. *Phys. Rev. E* **2016**, *93* (5), 052804.
- (7) Mechkov, S.; Cazabat, A. M.; Oshanin, G. Post-Tanner Stages of Droplet Spreading: The Energy Balance Approach Revisited. *J. Phys. Condens. Matter* **2009**, *21* (46), 464131.
- (8) Voinov, O. V. Hydrodynamics of Wetting. *Fluid Dyn.* **1977**, *11* (5), 714–721.
- (9) de Gennes, P. G.; H, H. Dynamique Du Mouillage: Films, Precurseurs Sur Solide “Sec.” *C.R. Acad. Sci. Paris Ser II* **1984**, No. 299, 499–503.
- (10) De Gennes, P. G. Wetting: Statics and Dynamics. *Rev. Mod. Phys.* **1985**, *57* (3), 827–863.
- (11) Mondal, P. K.; Ghosh, U.; Bandopadhyay, A.; DasGupta, D.; Chakraborty, S. Pulsating Electric Field Modulated Contact Line Dynamics of Immiscible Binary Systems in Narrow Confinements under an Electrical Double Layer Phenomenon. *Soft Matter* **2014**, *10* (42), 8512–8523.
- (12) Mondal, P. K.; DasGupta, D.; Bandopadhyay, A.; Ghosh, U.; Chakraborty, S. Contact Line Dynamics of Electroosmotic Flows of Incompressible Binary Fluid System with Density and Viscosity Contrasts. *Phys. Fluids* **2015**, *27* (3).
- (13) Mondal, P. K.; DasGupta, D.; Chakraborty, S. Rheology-Modulated Contact Line

- Dynamics of an Immiscible Binary System under Electrical Double Layer Phenomena. *Soft Matter***2015**, *11* (33), 6692–6702.
- (14) Agrawal, M. S.; Gaikwad, H. S.; Mondal, P. K.; Biswas, G. Analysis and Experiments on the Spreading Dynamics of a Viscoelastic Drop. *Appl. Math. Model.***2019**, *75*, 201–209.
 - (15) Rafai, S.; Bonn, D. Spreading of Non-Newtonian Fluids and Surfactant Solutions on Solid Surfaces. *Phys. A Stat. Mech. its Appl.***2005**, *358* (1 SPEC. ISS.), 58–67.
 - (16) Dandapat, B. S.; Singh, S. K. Spreading of a Non-Newtonian Liquid Drop over a Horizontal Plane. *Chem. Eng. Sci.***2010**, *65* (11), 3427–3430.
 - (17) Singh, S. K.; Dandapat, B. S. Spreading of a Non-Newtonian Liquid Drop over a Homogeneous Rough Surface. *Colloids Surfaces A Physicochem. Eng. Asp.***2013**, *419*, 228–232.
 - (18) Schimmele, L.; Napiórkowski, M.; Dietrich, S. Conceptual Aspects of Line Tensions. *J. Chem. Phys.***2007**, *127* (16), 164715.
 - (19) Wang, J. Y.; Betelu, S.; Law, B. M. Line Tension Approaching a First-Order Wetting Transition: Experimental Results from Contact Angle Measurements. *Phys. Rev. E***2001**, *63* (3), 031601.
 - (20) Berg, J. K.; Weber, C. M.; Riegler, H. Impact of Negative Line Tension on the Shape of Nanometer-Size Sessile Droplets. *Phys. Rev. Lett.***2010**, *105* (7), 076103.
 - (21) Widom, B. Line Tension and the Shape of a Sessile Drop. *J. Phys. Chem.***1995**, *99* (9), 2803–2806.
 - (22) Fan, H. Liquid Droplet Spreading with Line Tension Effect. *J. Phys. Condens. Matter***2006**, *18* (19), 4481–4488.
 - (23) Thien N. P.; Tanner R. I. A New Constitutive Theory Equation Derived from Network. *J. Nonnewton. Fluid Mech.***1977**, *2*, 353–365.
 - (24) Bird, R. B.; Stewart, W. E.; Lightfoot, E. N. *Transport Phenomena*, second.; John Wiley & Sons, Inc., 2006.
 - (25) Mondal, P. K.; Mukherjee, S. Thermodynamically Consistent Limiting Nusselt Number in the Viscous Dissipative Non-Newtonian Couette Flows. *Ind. Eng. Chem. Res.***2014**, *53* (1), 402–414.
 - (26) Ferrás, L. L.; Afonso, A. M.; Alves, M. A.; Nóbrega, J. M.; Pinho, F. T. Electro-Osmotic and Pressure-Driven Flow of Viscoelastic Fluids in Microchannels: Analytical and Semi-Analytical Solutions. *Phys. Fluids***2016**, *28* (9), 093102.
 - (27) Bejan, A. *Entropy Generation through Heat and Fluid Flow*; Wiley: New York, 1994.
 - (28) Baaijens, H. P. W.; Peters, G. W. M.; Baaijens, F. P. T.; Meijer, H. E. H. Viscoelastic Flow Past a Confined Cylinder of a Polyisobutylene Solution. *J. Rheol. (N. Y.)***1995**, *39* (6), 1243–1277. h
 - (29) Baaijens, F. P. T. Numerical Analysis of Start-up Planar and Axisymmetric Contraction Flows Using Multi-Mode Differential Constitutive Models. *J. Nonnewton. Fluid Mech.***1993**, *48* (1–2), 147–180..
 - (30) Quinzani, L. M.; Armstrong, R. C.; Brown, R. A. Birefringence and Laser-Doppler Velocimetry (LDV) Studies of Viscoelastic Flow through a Planar Contraction. *J. Nonnewton. Fluid Mech.***1994**, *52* (1), 1–36.
 - (31) Quinzani, L. M.; Armstrong, R. C.; Brown, R. A. Use of Coupled Birefringence and LDV Studies of Flow through a Planar Contraction to Test Constitutive Equations for Concentrated Polymer Solutions. *J. Rheol. (N. Y.)***1995**, *39* (6), 1201–1228.
 - (32) Iwamatsu, M. Line-Tension Effects on Heterogeneous Nucleation on a Spherical Substrate and in a Spherical Cavity. *Langmuir***2015**, *31* (13), 3861–3868.
 - (33) Reiner, M. The Deborah Number. *Phys. Today***1964**, *17* (1), 62–62.
 - (34) Bertrand, E.; Blake, T. D.; Coninck, J. De. Influence of Solid–Liquid Interactions on

- Dynamic Wetting: A Molecular Dynamics Study. *J. Phys. Condens. Matter***2009**, *21* (46), 464124.
- (35) Wang, X. D.; Zhang, Y.; Lee, D. J.; Peng, X. F. Spreading of Completely Wetting or Partially Wetting Power-Law Fluid on Solid Surface. *Langmuir***2007**, *23* (18), 9258–9262.